PDMS Composites with Photostable NIR Dyes for B-Mode Ultrasound Imaging

1st India Lewis Thompson
Dept. of Med. Phys. and Biomed. Eng.
University College London
London, UK
0000 − 0001 − 9662 − 6400

2nd Sunish Mathews
Dept. of Med. Phys. and Biomed. Eng.
University College London
London, UK
0000 − 0002 − 2289 − 3669

3rd Edward Zhang
Dept. of Med. Phys. and Biomed. Eng.
University College London
London, UK
0000 − 0003 − 3717 − 1367

4th Paul Beard
Dept. of Med. Phys. and Biomed. Eng.
University College London
London, UK
0000 − 0001 − 7710 − 2759

5th Adrien Desjardins
Dept. of Med. Phys. and Biomed. Eng.
University College London
London, UK
0000 − 0002 − 1932 − 1811

6th Richard Colchester
Dept. of Med. Phys. and Biomed. Eng.
University College London
London, UK
0000 − 0001 − 8657 − 0546

***Abstract*—All-optical ultrasound has rapidly progressed as an imaging paradigm well-suited to application in minimally invasive surgical scenarios, moving from benchtop to *in vivo* studies. In this work, we build on previous studies, demonstrating B-mode all-optical ultrasound imaging using a composite comprising a photostable near-infrared absorbing dye and polydimethylsiloxane. This composite is cost-effective and simple to manufacture, and capable of generating broadband (*ca.* 35 MHz) and high-pressure (*ca.* 1.5 MPa) ultrasound. The composite was compared with an established ultrasound-generating composite: reduced graphene oxide with polydimethlysiloxane. Both materials were coated on multimode optical fibres and were optically and ultrasonically characterized. Further, the transmitters were coupled with a plano-concave microresonator for ultrasound reception and synthetic aperture B-mode pulse-echo US imaging of a tungsten wire phantom and *ex vivo* swine aorta tissue was performed. The images acquired using each transmitter were compared in terms of the image resolution and signal-to-noise ratio.**

***Index Terms*—ultrasound, fibre optic, PDMS, NIR dyes, all-optical ultrasound**

I. Introduction

All-optical ultrasound (OpUS) is a pulse-echo imaging technique that uses light to both generate and receive ultrasound, which has demonstrated broadband emission, high sensitivities, and high miniaturisability [1–3]. With this technique, ultrasound is generated via absorption of pulsed or modulated light in a coating material. This leads to a temperature rise and corresponding pressure change via the photoacoustic effect which propagates as an ultrasound wave [4]. Ultrasound reception can be achieved optically using interferometric sensors such as plano-concave microresonators [5] or microring resonators [6]. The all-optical imaging system is completed using one optical fibre for ultrasound transmission and a second for reception.

Composite coatings comprising elastomeric and absorbing components have emerged as efficient optical transducers. A wide variety of absorbers have been studied, including metallic nanostructures [1, 7], graphene [8], candle soot [9, 10] and carbon nanotubes [11–13]. Typically, polydimethylsiloxane (PDMS) is used as an elastomeric host component due to its large thermal expansion coefficient, which provides efficient photoacoustic conversion [1, 8, 10, 14].

This research was supported by the the Royal Academy of Engineering under the Research Fellowship Scheme (RF/201819/18/125) and the Wellcome/EPRSC Centre for Interventional and Surgical Sciences (203145/Z/16/Z).

To date, ultrasound generating composites deposited on the tips of optical fibres have enabled imaging in both two- [15] and three- [16] dimensions as well as real-time *in vivo* M-mode imaging [3], proving the feasibility of OpUS for minimally invasive imaging. One area of interest is the development of wavelength-selective composite coatings for incorporation of complementary optical modalities [17]. Here, the ultrasound can be generated at one wavelength via optical absorption within the coating, whilst at other wavelengths light can be transmitted through the coating and be used for a complementary modality such as photoacoustic imaging [7, 18] or ablation [14].

Previous research into wavelength-selective composites includes optical absorbers such as crystal violet or gold nanoparticles embedded in PDMS [1]. However, these composites suffered from poor photostability under prolonged laser exposure and limited ultrasound pressures and bandwidths, respectively. More recently, quantum dots have been demonstrated for co-registered ultrasound and photoacoustic imaging, but the quantum dots were synthesised through a complex process [17]. Thus, there is a need for a wavelength-selective composite which can be fabricated through facile fabrication methods whilst still providing high bandwidth and high pressure ultrasound.

This work builds on previous research which introduced Epolight 9837 as an optical absorber for optical ultrasound generation [19]. In this study, an Epolight-PDMS composite coating was compared with an established reduced graphene oxide (rGO)-PDMS composite [8] and B-mode imaging was demonstrated.

II. Methods

A. Fabrication

OpUS transmitters comprising a near-infrared (NIR) dye (Epolight 9837, Epolin, UK) as an optical absorber and PDMS as an elastomeric host were developed. Comparative transmitters were manufacted using a previously demonstrated rGO-PDMS composite [8].

Optical fibres (fused silica core/cladding, core diameter: 400 µm, FG400LEP, Thorlabs, UK) were prepared for coating by removing the buffer coating from the distal end of the fibre. Subsequently, the distal end was cleaved manually using a tungsten blade. Each of the optical absorbers were prepared prior to the first coating layer. The rGO was prepared as outlined in [8]; 500 mg of rGO functionalised with octadecylamine (805084, Sigma Aldrich, UK) was sonicated for 20 s in 2.5 ml of xylene to give a homogeneous solution. The Epolight was

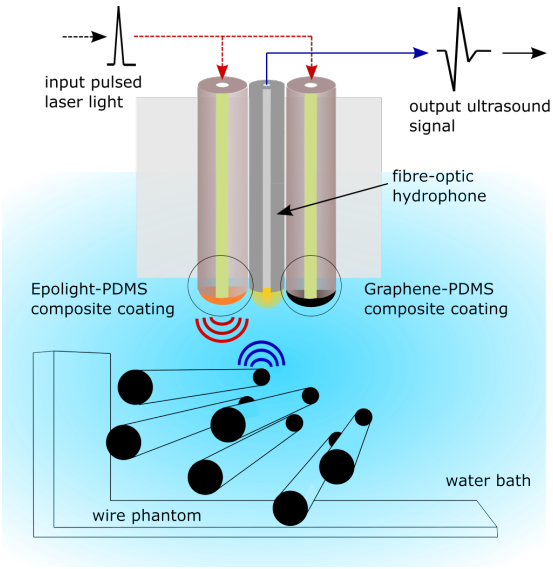

Fig. 1. Schematic of fibre arrangement for B-mode imaging.

prepared by sonicating 15 mg of dry dye in 0.5 ml of xylene for 30 s to facilitate dispersion. The cleaved face of the prepared optical fibres were then dipped into the respective optical absorbers and removed, leaving a thin film on the fibre surface. This layer of absorber was left to dry in ambient conditions for *ca.* 24 hours. Subsequently, both types of optical absorber were overcoated with a solution comprising a solution of PDMS (MED-1000, Polymer Systems Technology, UK) diluted with xylene (ratio 250 mg PDMS: 0.5 ml xylene) to reduce the viscosity. The coated optical fibres were left to cure under ambient conditions for 24 hours with the distal surface facing up.

B. Characterisation

The coated fibres were examined visually using a stereo-microscope. Subsequently, the optical absorption for both the Epolight-PDMS and graphene-PDMS composite coated fibres was measured over the wavelength range $400-1700$ nm using two spectrometers (Flame ($400-900$ nm) & NIRQuest512 ($800-1800$ nm), Ocean Optics, USA) and an integrating sphere.

The generated ultrasound was characterised by coupling a pulsed Nd:YAG laser (wavelength: 1064 nm, pulse width: 2 ns, repetition rate: 100 Hz, Spot-10-500-1064, Elforlight, UK) into the fibre under test. The laser had a pulse energy of 20 µJ, corresponding to an incident fluence of 15.9 mJ/cm^2 on the composite coating. The generated ultrasound was measured at a distance of 1.5 mm from the coating using a 200 µm needle hydrophone (Precision Acoustics, UK) with a calibrated range $1-30$ MHz. The acquired time-series were Fourier transformed and the hydrophone calibration was applied to obtain the ultrasound bandwidth.

C. B-Mode Imaging

1) Data Acquisition: The fabricated transmitters were affixed adjacent to a plano-concave microresonator to provide ultrasound generation and reception, respectively (Fig.1). This probe was then clamped to a motorised stage (MTS50/M-Z8, Thorlabs, UK) controlled by a motor controller (TDC001 T-Cube DC, Thorlabs, UK). The transmitters were coupled to the pulsed Nd:YAG laser for ultrasound generation (1064 nm, Elforlight, UK).

The plano-concave microresonator was interrogated with a continuous wave laser (Tunics T100S-HP, Yenista Optics, France) with a tuning range of $1500-1630$ nm and a power of 4.5 mW as described in previous studies [8, 14]. The laser was connected via a fibre optic circulator which allowed the reflected signal to be detected with a photoreceiver. The photoreceiver split the signal into high-frequency ($>$ 500 kHz) and low-frequency ($<$ 50 kHz) components. The low-frequency component was digitised at 16 bits (PCI-6251, National Instruments, UK) and was used to record the transfer function of the microresonator and estimate the optimum bias point. The high-frequency component was digitised at 14 bits with a sample rate of 100 MS/s (PCI-5142, National Instruments, UK) and was used to record the modulation of the reflection induced by the incident acoustic wave. The sensor was biased to the point of the maximum derivative of the interferometer transfer function of the plano-concave microresonator to optimise the sensitivity [20].

Imaging was performed by translating the probe one horizontal step at a time using the motorised stage and acquiring an A-line at each step. Each A-line consisted of 4000 sensor data points corresponding to a depth of *ca.* 30 mm. The A-lines were then concatenated to form a complete data set. Imaging was performed sequentially with the comparative transmitters; each scan using the Epolight-PDMS transmitter was immediately repeated with the rGO-PDMS transmitter to ensure direct comparison.

2) Image Processing: The data was high pass filtered (4th order Butterworth) with a cut-off frequency of 40 MHz. A cross-talk algorithm was applied [15], followed by image reconstruction using the k-Wave toolbox [21]. Briefly, for image reconstruction, a fast Fourier transform was computed on both dimensions (t, y) converting the raw data to wavenumber-frequency space. Subsequently, the data was then mapped to wavenumber-wavenumber space using the dispersion relation for a plane wave. Finally, an inverse Fourier transform was then computed back to the spatial domain (x, y). The signal envelope was found using the absolute value of the Hilbert transform followed by a log transformation.

3) Imaging Targets: A custom phantom comprising a series of parallel tungsten wires (D:27 µm) mounted on a plastic frame was used to assess the imaging resolution. This phantom appears in reconstructed images as a series of point-spread-functions (PSF) which can be used to measure the resolution of the imaging system. The imaging targets were fixed in position in a water bath (Fig.1), while the OpUS probe was translated relative to the target. Data acquisition was carried out using A-line spacings of $25-200$ µm. For each of the reconstructed images, the axial and lateral resolution were calculated as the full-width half-maximum (FWHM) values of the PSFs that represented the tungsten wires in the images.

Imaging of *ex vivo* swine aorta tissue (Medmeat, UK) was carried out to ascertain the potential for visualising biological structures. In preparation for imaging the vessels were cut parallel to their longitudinal axis and fixed to a cork mount with the inner surface facing up towards the ultrasound probe. The cork mount and tissue were placed in the water bath.

III. Results

A. Characterisation

The microscope images were examined for coating uniformity and thickness (Fig.2a-b). Fibres with excessively thick coating layers ($>$ 0.15 mm) or visible agglomerations of optical absorber were eliminated prior to characterisation.

The rGO and Epolight dyes exhibited different optical absorption profiles (Fig.2c). The Epolight composite exhibited an optical absorption peak of *ca.* 95% at *ca.* $900-1100$ nm while demonstrating

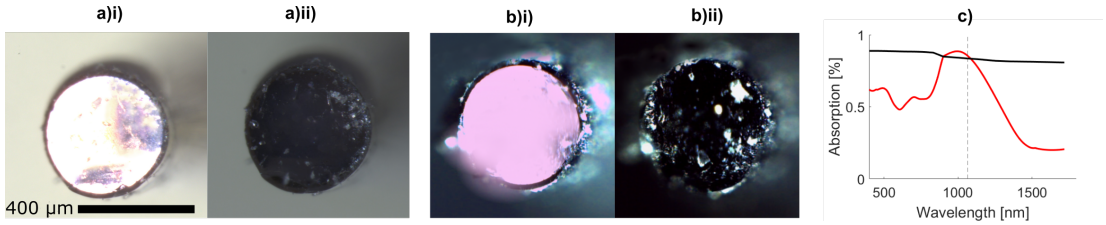

Fig. 2. a) Stereo-microscope image of distal face of Epolight-PDMS transmitter i) with through-illumination and ii) unlit. Scale bar: 400 µm. b) Distal face of rGO-PDMS transmitter i) with through illumination and ii) unlit. c) Optical absorption spectra of Epolight-PDMS (red line) and rGO-PDMS (black line).

$< 30\%$ absorption at wavelengths > 1100 nm and *ca.* 50% absorption at wavelengths < 900 nm. The rGO composite, in comparison, exhibited a broadband absorption of *ca.* $90\% \pm 5\%$ at all wavelengths.

The Epolight-PDMS composite exhibited peak-to-peak ultrasound pressure of 1.7 MPa (Fig.3a)i)) with corresponding -6 dB ultrasound bandwidths 35 MHz (Fig.3b). In comparison, the graphene-PDMS composite generated ultrasound pressures of 1.3 MPa (Fig.3a)ii)) with a bandwidth of 32 MHz (Fig.3b).

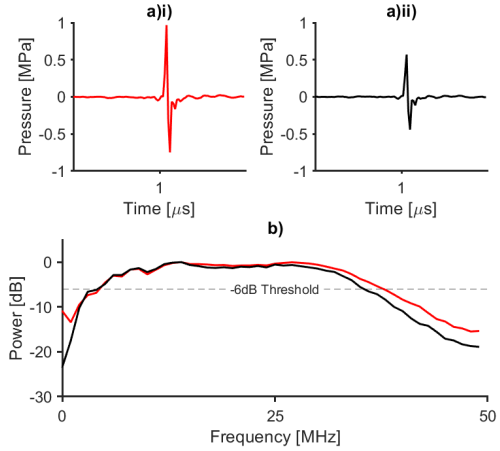

Fig. 3. a) Transmitted ultrasound time-series measured at 1.5 mm for (i) Epolight-PDMS and (ii) graphene-PDMS coatings. b) Corresponding ultrasound power spectrum.

B. Resolution Study

All phantom PSFs were visible in the ultrasound images acquired by both the Epolight-PDMS and rGO-PDMS transmitters (Fig.4a,b). The signal-to-noise (SNR) was highest for the tungsten wires closest to the probe (Epolight: 40 dB, rGO: 38 dB). The contrast of the PSF decreased with depth by *ca.* 2 dB/mm (Fig.4c).

It was found that decreasing the A-line acquisition step-size improved the resolution. In particular, the lateral resolution given by the Epolight-PDMS transmitter improved from 200 µm to 60 µm at a depth of 4 mm as the spacing was reduced from 200 µm to 50 µm (Fig.4e). This relationship was also observed in the lateral resolution given by the rGO-PDMS transmitter at decreasing acquisition step-size.

For all images, the lateral resolution deteriorated with depth (Fig.4e),g). The best resolution was found at 4 mm (Epolight-PDMS: 60 µm, rGO-PDMS: 75 µm), while the larger depths of 25 mm showed poorer resolutions (Epolight-PDMS: 120 µm, rGO-PDMS: 110 µm) at a maintained A-line spacing of 25 µm.

The axial resolution remained relatively constant at all depths and A-line step-sizes (50 ± 8 µm) (Fig.4d),f).

C. Swine Aorta

The aorta tissue surface was visible in the OpUS images throughout acquisition. For *ex vivo* images, the vessel was well-resolved and the cork mount behind the vessel could be visualised. For both the Epolight-PDMS (Fig.5a) and rGO-PDMS (Fig.5b) composites, three layers were visible in the vessel wall in the reconstructed OpUS images. These were thought to correspond to the intima (represented by a bright region indicated by a green arrow), the media (indicated by a blue arrow) and adventitia (indicated by a purple arrow). Further visible features included the side branches (yellow arrows) and cork mount (pink arrow). The Epolight-PDMS transmitter generated a peak SNR *ca.* 35 dB. The rGO-PDMS transmitter, in comparison, demonstrated a peak SNR *ca.* 25 dB.

IV. Discussion

Here, we present an OpUS device for B-mode imaging using a photostable NIR dye as an optical absorber. After both optical and acoustic characterisation, this transmitter was used in conjunction with a plano-concave microresonator for ultrasound imaging and compared to previously-presented rGO-PDMS transmitters. A bench-top all-optical ultrasound imaging setup was used to acquire 2D images with resolutions as low as 75 µm laterally and 50 µm axially. Tissue images were well-resolved with structures clearly visualised.

The peak-to-peak pressure and bandwidth of the two composites studied here are relatively similar: pressures in excess of 1.3 MPa and corresponding -6 dB bandwidths *ca.* 35 MHz. The small difference in the generated ultrasound pressure is likely due to the difference in the optical spectra; Epolight absorbed 95% at the incident wavelength whereas rGO absorbed 89%.

As with conventional ultrasound imaging, axial resolution is typically limited by the bandwidth of the both the generated ultrasound and the ultrasound receiver [22]. Optical ultrasound generation can achieve wide transmission bandwidths with the use of short laser excitation pulses [23]. Since the brevity of the excitation pulse is not altered through the change in acquisition step-size, it would be expected that the axial resolution remains constant with change step-size. However, whilst a short pulse length will contribute to a higher axial resolution, this will reduce the penetration depth in tissue due to the higher attenuation of high ultrasound frequencies. This may be responsible for the slight upward in axial resolution found with the rGO-PDMS transmitters (Fig.4f) from > 20 mm). This was not found with the Epolight-PDMS transmitter (Fig.4d), likely due to the larger peak-to-peak pressure generated by this transmitter, leading to greater pressure at higher depths.

Lateral resolution is dictated by the width of the ultrasound beam and the bandwidth of the ultrasound [22], as well as the width of the synthetic aperture and element spacing. The narrow aperture size of the ultrasound generating elements will lead to a divergent beam which is optimal when image reconstruction is used and

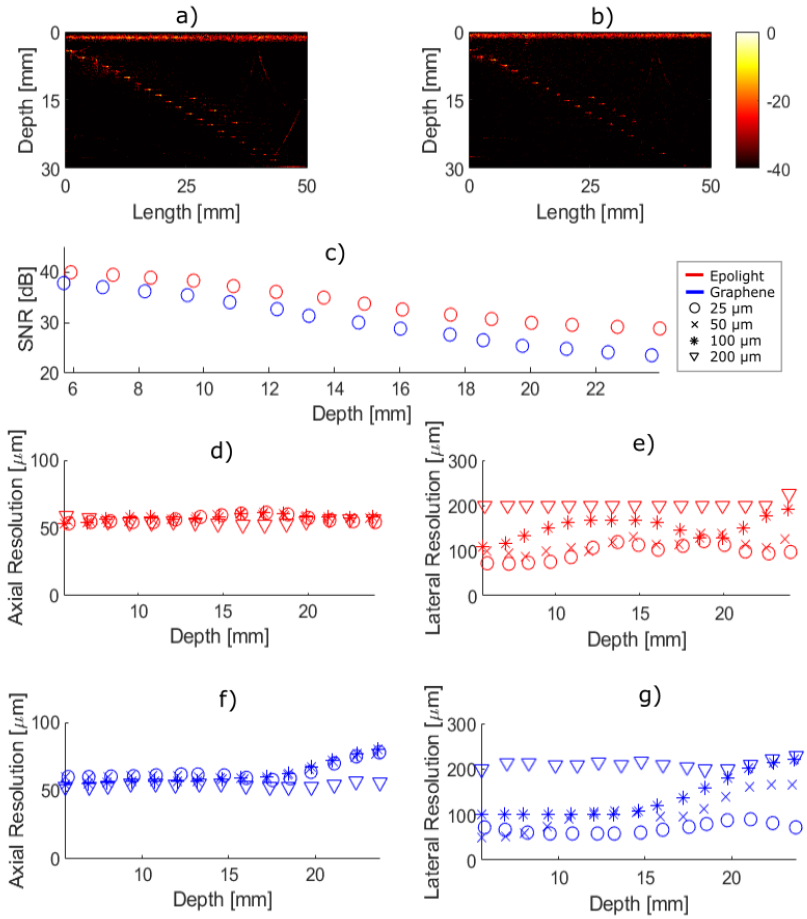

Fig. 4. B-mode optical ultrasound images of custom 27 µm resolution phantom using a Fabry-Perot hydrophone in conjunction with a) Epolight-PDMS transmitter and b) graphene-PDMS transmitter. c) SNR measurements over depth. d) Axial and e) lateral ultrasound resolutions for the Epolight-PDMS transmitter. f) Axial and g) lateral ultrasound resolutions for the graphene-PDMS transmitter.

was consistent between the two comparative transmitters, thus any variation in lateral resolution should be proportional to the variation in the bandwidth of the generated ultrasound. The lateral resolution values are comparable to a typical commercial ultrasound device which can achieve lateral resolutions of 100 µm depending on the bandwidth and frequency of the device [22]. The quality of the lateral resolution was indicated to be inversely proportional to the acquisition step-size. This compromise between resolution and step-size is necessary to quantify prior to further pre-clinical studies in order to minimise the computationally intensive reconstruction while allowing detailed images of large areas. Figures 4(e) and 4(g) show a similar lateral resolution over depth at 25 and 50 µm step-sizes, thereby maintaining comparable resolution while halving the collected data set.

Ex vivo swine aorta tissue was imaged, showing peak SNR of 35 dB and clear distinction of tissue layers. These images exhibited a higher SNR than those obtained with the rGO-PDMS transmitter, but were comparable in terms of the tissue layer distinction and side branch identification. Accurate identification of tissue layers would necessitate a histological study which was not performed. As such, the tissue layers were identified from previous similar studies such as [15]. Detailed comparisons to histological analyses would be valuable to ascertain the detail quality in the reconstructed images and therefore the future application of Epolight-PDMS transmitters to medical imaging. In particular, concurrent histological studies and OpUS images of tissues encountered in other clinical contexts that have previously been studied with fluorescence or photoacoustic imaging, such as lung [24] or gastrointestinal tissue [25], will be valuable in the assessment of the OpUS component of multimodal imaging using Epolight-PDMS transmitters.

It is expected that follow-up studies will be carried out incorporating complementary modalities through the wavelength-selective absorption profile demonstrated by this composite. The comparable imaging parameters demonstrated by this system with both the previously presented transmitter and conventional piezoelectric ultrasound is indicative of the potential of this composite material in an OpUS application. The selective nature of the narrow absorption window at 1064 nm gives the opportunity for both short wavelength modalities such as ablation [26] and photoacoustic imaging [27] and long wavelength modalities such as fluorescence imaging using Indium-based contrast agents [28].

Data Availability

The datasets generated during and/or analysed during the current study are available from the corresponding author upon reasonable

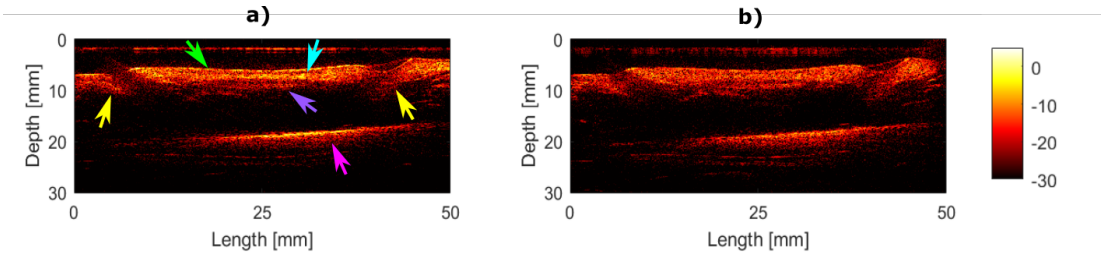

Fig. 5. B-mode optical ultrasound images of *ex vivo* swine aorta tissue acquired using a) Epolight-PDMS transmitters and b) graphene-PDMS transmitters.

request.

REFERENCES

[1] S Noimark, RJ Colchester, RK Poduval, E Maneas, EJ Alles, T Zhao, EZ Zhang, M Ashworth, E Tsolaki, AH Chester, et al. Polydimethylsiloxane composites for optical ultrasound generation and multimodality imaging. *Advanced Functional Materials*, 28(9):1704919, 2018.

[2] RJ Colchester, C Little, G Dwyer, S Noimark, EJ Alles, EZ Zhang, CD Loder, IP Parkin, I Papakonstantinou, PC Beard, et al. All-optical rotational ultrasound imaging. *Scientific Reports*, 9(1):1–8, 2019.

[3] MC Finlay, CA Mosse, RJ Colchester, S Noimark, EZ Zhang, S Ourselin, PC Beard, RJ Schilling, IP Parkin, I Papakonstantinou, et al. Through-needle all-optical ultrasound imaging *in vivo*: a preclinical swine study. *Light: Science & Applications*, 6(12):e17103–e17103, 2017.

[4] BT Cox and PC Beard. Fast calculation of pulsed photoacoustic fields in fluids using k-space methods. *The Journal of the Acoustical Society of America*, 117(6):3616–3627, 2005.

[5] EZ Zhang and PC Beard. A miniature all-optical photoacoustic imaging probe. In *Photons plus Ultrasound: Imaging and Sensing*, volume 7899, page 78991F. International Society for Optics and Photonics, 2011.

[6] S Ashkenazi, CY Chao, LJ Guo, and M O'donnell. Ultrasound detection using polymer microring optical resonator. *Applied Physics Letters*, 85(22):5418–5420, 2004.

[7] D Cui, Z Zhang, and Y Shi. Optically-excited simultaneous photoacoustic and ultrasound imaging based on a flexible gold-PDMS film. *Journal of Innovative Optical Health Sciences*, 13(04):2050012, 2020.

[8] RJ Colchester, EJ Alles, and AE Desjardins. A directional fibre optic ultrasound transmitter based on a reduced graphene oxide and polydimethylsiloxane composite. *Applied Physics Letters*, 114(11):113505, 2019.

[9] J Kim, WY Chang, H Wu, and X Jiang. Optical fiber laser-generated-focused-ultrasound transducers for intravascular therapies. In *2017 IEEE International Ultrasonics Symposium (IUS)*, pages 1–4. IEEE, 2017.

[10] WY Chang, W Huang, J Kim, S Li, and X Jiang. Candle soot nanoparticles-polydimethylsiloxane composites for laser ultrasound transducers. *Applied Physics Letters*, 107(16):161903, 2015.

[11] G Yoo, H Yoon, J Heo, UjK Thakur, HJ Park, HW Baac, and J Heo. All-optical ultrasound transducer using CNT-PDMS and etalon thin-film structure. *IEEE Photonics Journal*, 7(6):1–8, 2015.

[12] RJ Colchester, CA Mosse, DS Bhachu, JC Bear, CJ Carmalt, IP Parkin, BE Treeby, I Papakonstantinou, and AE Desjardins. Laser-generated ultrasound with optical fibres using functionalised carbon nanotube composite coatings. *Applied Physics Letters*, 104(17):173502, 2014.

[13] EJ Alles, J Heo, S Noimark, RJ Colchester, IP Parkin, HW Baac, and AE Desjardins. Acoustical characterisation of carbon nanotube-loaded polydimethylsiloxane used for optical ultrasound generation. In *2017 IEEE International Ultrasonics Symposium (IUS)*, pages 1–4. IEEE, 2017.

[14] S Zhang, EZ Zhang, PC Beard, AE Desjardins, and RJ Colchester. Dual-modality fibre optic probe for simultaneous ablation and ultrasound imaging. *Communications Engineering*, 1(1):1–9, 2022.

[15] RJ Colchester, EZ Zhang, CA Mosse, PC Beard, I Papakonstantinou, and AE Desjardins. Broadband miniature optical ultrasound probe for high resolution vascular tissue imaging. *Biomedical Optics Express*, 6(4):1502–1511, 2015.

[16] JA Guggenheim, J Li, TJ Allen, RJ Colchester, S Noimark, O Ogunlade, IP Parkin, I Papakonstantinou, AE Desjardins, EZ Zhang, et al. Ultrasensitive plano-concave optical microresonators for ultrasound sensing. *Nature Photonics*, 11(11):714–719, 2017.

[17] S Bodian, RJ Colchester, TJ Macdonald, F Ambroz, M Briceno de Gutierrez, SJ Mathews, YMM Fong, E Maneas, KA Welsby, RJ Gordon, et al. Cuins2 quantum dot and polydimethylsiloxane nanocomposites for all-optical ultrasound and photoacoustic imaging. *Advanced Materials Interfaces*, page 2100518, 2021.

[18] BY Hsieh, SL Chen, T Ling, LJ Guo, and PC Li. All-optical transducer for ultrasound and photoacoustic imaging by dichroic filtering. In *2012 IEEE International Ultrasonics Symposium*, pages 1410–1413. IEEE, 2012.

[19] S Zhang, S Noimark, AE Desjardins, and RJ Colchester. PDMS composites with photostable NIR dyes for multi-modal ultrasound imaging. *MRS Advances*, pages 1–5, 2022.

[20] E Zhang, J Laufer, and P Beard. Backward-mode multiwavelength photoacoustic scanner using a planar fabry-perot polymer film ultrasound sensor for high-resolution three-dimensional imaging of biological tissues. *Applied Optics*, 47(4):561–577, 2008.

[21] BE Treeby and BT Cox. k-wave: Matlab toolbox for the simulation and reconstruction of photoacoustic wave fields. *Journal of Biomedical Optics*, 15(2):021314, 2010.

[22] A Ng and J Swanevelder. Resolution in ultrasound imaging. *Continuing Education in Anaesthesia Critical Care & Pain*, 11(5):186–192, 2011.

[23] D Menichelli and E Biagi. Optoacoustic sources: a practical green function-based model for thin film laser-ultrasound generation. *Journal of Optics A: Pure and Applied Optics*, 3(4):S23, 2001.

[24] C Lee, K Fujino, Y Motooka, A Gregor, N Bernards, H Ujiie, T Kinoshita, K Chung, S Han, and K Yasufuku. Photoacoustic imaging to localize indeterminate pulmonary nodules: A preclinical study. *PloS one*, 15(4):e0231488, 2020.

[25] Zhaojun Nie, Shu-Chi Allison Yeh, Michelle LePalud, Fares Badr, Frances Tse, David Armstrong, Louis WC Liu, M Jamal Deen, and Qiyin Fang. Optical biopsy of the upper GI tract using fluorescence lifetime and spectra. *Frontiers in Physiology*, 11:339, 2020.

[26] SS Zakariyah, PP Conway, DA Hutt, DR Selviah, K Wang, J Rygate, J Calver, and W Kandulski. Fabrication of polymer waveguides by laser ablation using a 355 nm wavelength nd: Yag laser. *Journal of Lightwave Technology*, 29(23):3566–3576, 2011.

[27] M Gandolfi, F Banfi, and C Glorieux. Optical wavelength dependence of photoacoustic signal of gold nanofluid. *Photoacoustics*, 20:100199, 2020.

[28] L Shi, LA Sordillo, A Rodríguez-Contreras, and R Alfano. Transmission in near-infrared optical windows for deep brain imaging. *Journal of Biophotonics*, 9(1-2):38–43, 2016.